

ACCEPTED VERSION

Shaun Fitzgerald, Richard Kelso, Paul Grimshaw, Andrew Warr

Measurement of the air velocity and turbulence in a simulated track cycling team pursuit race

Journal of Wind Engineering and Industrial Aerodynamics, 2019; 190:322-330

© 2019 Elsevier Ltd. All rights reserved.

This manuscript version is made available under the CC-BY-NC-ND 4.0 license

<http://creativecommons.org/licenses/by-nc-nd/4.0/>

Final publication at <http://dx.doi.org/10.1016/j.jweia.2019.05.014>

PERMISSIONS

<https://www.elsevier.com/about/policies/sharing>

Accepted Manuscript

Authors can share their [accepted manuscript](#):

24 Month Embargo

After the embargo period

- via non-commercial hosting platforms such as their institutional repository
- via commercial sites with which Elsevier has an agreement

In all cases [accepted manuscripts](#) should:

- link to the formal publication via its DOI
- bear a CC-BY-NC-ND license – this is easy to do
- if aggregated with other manuscripts, for example in a repository or other site, be shared in alignment with our [hosting policy](#)
- not be added to or enhanced in any way to appear more like, or to substitute for, the published journal article

5 July 2021

<http://hdl.handle.net/2440/125729>

Title: Measurement of the air velocity and turbulence in a simulated track cycling team pursuit race.

Authors: Shaun Fitzgerald ^{*a}, Richard Kelso ^a, Paul Grimshaw ^a and Andrew Warr ^b

Affiliations:

^a School of Mechanical Engineering, The University of Adelaide, Adelaide, SA 5005, Australia

^b Australian Institute of Sport, Bruce, ACT 2617, Australia

Author Contact Details:

Shaun Fitzgerald

Address: School of Mechanical Engineering, The University of Adelaide, Adelaide, SA 5005, Australia

E-mail: shaun.fitzgerald@adelaide.edu.au

Associate Professor Richard Kelso

Address: School of Mechanical Engineering, The University of Adelaide, Adelaide, SA 5005, Australia

E-mail: richard.kelso@adelaide.edu.au

Associate Professor Paul Grimshaw

Address: School of Mechanical Engineering, The University of Adelaide, Adelaide, SA 5005, Australia

E-mail: paul.grimshaw@adelaide.edu.au

Andrew Warr

Address: Australian Institute of Sport, Bruce, ACT 2617, Australia

E-mail: a.warr@cycling.org.au

Corresponding Author: Shaun Fitzgerald

Declarations of interest: none.

24 Abstract

25 There are many cycling events undertaken in a velodrome which involve close interactions between cyclists.
26 During a single race, particularly the team pursuit, a cyclist can alternately be ahead of or behind another rider;
27 two positions which have very different flow fields. Additionally, as a cyclist travels around a level corner, the
28 relative flow experienced by the cyclist becomes curved. Due to the lean angle of the cyclist, this resolves into
29 a change in both the yaw and pitch angle as well as the flow speed relative to the cyclist. An experimental
30 investigation was conducted with a bicycle fitted with a three-component velocity probe placed anterior to
31 the rider in a simulated team pursuit race. The results demonstrate a reduction in the airspeed-to-wheel speed
32 ratio for each drafting cyclist, down to 46% for the 4th rider. The turbulence intensity increased for each
33 drafting position, from 1.5% to 18.5%. A yaw angle of up to 7° and pitch angle of -3° were observed on the
34 velodrome bends. In addition, a fluctuation in the yaw angle due to the cadence cycle was observed. The
35 results demonstrate the aerodynamic conditions experienced in track cycling and can be used to inform
36 further investigations.

37 **Keywords:** Cycling aerodynamics; wind turbulence; drag; cornering

38 1. Introduction

39 At typical race speeds, aerodynamic drag accounts for greater than 90% of the total resistive force on a cyclist
40 and the power required to maintain a constant speed is proportional to the velocity cubed (Kyle and Burke
41 1984). Numerous methods have been proposed to reduce the aerodynamic drag of a cyclist, both in the
42 academic literature and in industry (Crouch et al. 2017). However, the majority of these studies have been
43 conducted with a number of assumptions on the aerodynamic environment experienced by the cyclist and
44 bicycle, most notably for track cycling being that the only component of airflow is a direct headwind equal to
45 the cyclists' velocity. However, if there is an external factor affecting the airflow, then there will be an angle
46 of incidence between the airflow relative to the cyclist and their direction of travel. This angle can be split into
47 two components; the yaw and pitch angles, where yaw is the angle between the direction of motion and the
48 relative wind in the transverse (xy) plane, and pitch is the angle in the sagittal (xz) plane, both shown in Figure
49 1.

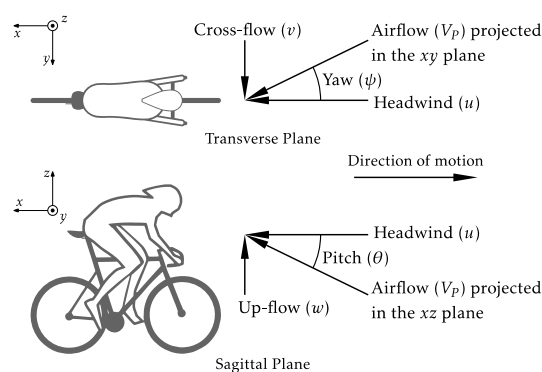


Figure 1. The three components (u, v, w) of total air velocity (V_p) and the yaw (ψ) and pitch (θ) angle definitions. The xyz coordinates are defined relative to the cyclist.

50 During outdoor cycling, yawed airflow typically occurs as a result of a natural cross wind; however, within an
51 indoor velodrome there is no natural wind and the current industry standard is to assume there is no yawed
52 or pitched airflow (Lukes et al. 2012, Underwood 2012, Caddy et al. 2017). This assumption greatly simplifies
53 the aerodynamic analysis of track cycling but it may not accurately model the realistic situation, as shown in a
54 study by Kyle (2003) where the airflow around a velodrome was observed by recording the wind angle anterior
55 to the handlebars of a bicycle as it traversed a track. Kyle (2003) proposes that this yaw angle arises due to the
56 bicycle turning on a track, shifting the incoming wind direction and causing a yawed flow relative to the bicycle
57 as the track curves. To the best of the authors' knowledge there have been no other previous studies on the

airflow experienced by a cyclist during cornering. Similar work has been completed in the automotive field on the effects of cornering, notably by Keogh et al. (2016) who completed a Computational Fluid Dynamics (CFD) analysis of curved airflow over a generic vehicle four-wheeled (Ahmed) body. Comprehensive studies on the wake of a single cyclist have been completed by a number of groups (Crouch et al. 2014, Crouch et al. 2016, Terra et al. 2019), however these studies have all been completed in a wind tunnel with straight, consistent airflow. The study by Keogh et al. (2016) on an Ahmed body demonstrated a significant difference in the flow field and aerodynamic forces due to the influence of curved airflow over the length of the vehicle body. Whilst there are obvious differences in the geometry and lean angle for a vehicle body compared to a cyclist, the clear differences in the wake for curved flow compared to straight flow demonstrates the requirement to accurately model the true aerodynamic conditions.

The effects of yawed airflow on the aerodynamic drag of a cyclist has previously been studied by Íñiguez-de-la-Torre and Íñiguez (2005) who found that with an increasing crosswind there was an increase in the drag force on a cyclist. These authors assumed a constant coefficient of drag and frontal area (i.e. constant $C_D A$) for all yaw angles, but this may not accurately replicate the true conditions where the $C_D A$ for a cyclist can be highly dependent on the yaw angle (Barry et al. 2012, Fintelman et al. 2015) and the total drag could decrease at higher yaw angles due to a lower $C_D A$.

Previous studies in cycling have used wind tunnels or CFD codes with low turbulence intensity, namely 0.2% (Blocken et al. 2018a, Blocken et al. 2018b), 0.5% (Terra et al. 2019), 1.4% and 1.6% (Crouch et al. 2014). However, there is often little discussion about why these values were chosen, and the true turbulence levels experienced by a cyclist on the road or in a velodrome have not been measured. The measurement and replication of turbulence is an area that has been extensively studied in other contexts, such as wind engineering where an understanding of the atmospheric boundary layer has been an industry standard for decades, and in vehicle aerodynamics where the turbulence relative to a moving vehicle has been extensively studied (Cooper and Watkins 2007). However there is a lack of turbulence measurements in regards to sports, an exception being work by Watkins and Alam (2014) who provide a theoretical review of possible sources of turbulence. Crouch et al. (2017) also mention that the turbulent flow field inside a velodrome is not well understood and could arise from natural or forced convection and the wakes of other cyclists. This could have an impact on many techniques for reducing the aerodynamic drag of a cyclist which involve 'tripping' the boundary layer into turbulence where the effects of freestream turbulence are known to induce this transition at lower speeds (Crouch et al. 2017).

A series of studies investigated the effects of turbulence on the drag of speed skaters on a skating rink using a three-component velocity probe (D'Auteuil 2010, D'Auteuil et al. 2012). In these investigations it was found that the airflow around a speed-skating rink is highly turbulent and there are components of yawed airflow relative to the skater around the corners. These authors describe a turbulent flow created by the skaters circling the track. This turbulence is caused by the skaters, structures surrounding and inside the track, and the temperature gradient from the surface of the ice. D'Auteuil et al. (2012) replicated their characterised on-track turbulence in a wind tunnel and observed a significant difference in the drag force on a mannequin in turbulent flow compared to smooth flow, highlighting the importance of correctly measuring and replicating the flow conditions. Track cycling operates in a similar environment and Reynolds number regime to speed skating and, with the exception of the temperature gradient due to ice, is likely to induce a similar turbulent flow pattern around the track.

Extensive work on the influence of drafting on the reduction of aerodynamic drag for a cyclist has been completed by previous authors for two cyclists (Blocken et al. 2013, Barry et al. 2016), four cyclists (Defraeye et al. 2014, Barry et al. 2015, Fitton et al. 2018), or more up to a full peloton (Blocken et al. 2018a, Blocken et al. 2018b). For a comprehensive review of the effects of drafting see Fitton et al. (2018) and Crouch et al. (2017). Work on the influence of a cyclist's posture and position within a group has been completed by Defraeye et al. (2014) who observed a difference in drag reduction dependent upon the relative position of different riders. An experimental study was completed on the wake interactions between two tandem cyclists by Barry et al. (2016) who found that the wake behind a second cyclist maintains strong similarity to that of a

single cyclist for large separation distances and deviates from the single cyclist wake for close separation, largely regardless of leg position. Work has also been completed for a pace line of up to 9 riders by Blocken et al. (2018a) who demonstrated a decreasing drag force from the 1st to 4th rider before the relative drag plateaus and all riders from 5th to 9th have a very similar drag force. A limitation in all of these studies on drafting is that they only consider a simple headwind equal to the cyclist's speed. If a crosswind is present then the drafting effect is likely to be reduced due to the wake from the leading cyclist being offset by the yaw angle, limiting the aerodynamic shelter provided to the trailing riders. This is observed in work by Belloli et al. (2016) who measured the drag of two cyclists for yaw angles of 0°, 3° and 5° and found a diminishing drag reduction effect at increasing yaw angles.

To the best of the authors' knowledge, there have been no previous studies that measure the aerodynamic flow field anterior to a cyclist in-situ during a team pursuit event inside a velodrome. The present study aims to investigate the aerodynamic conditions experienced by a track cyclist in order to further our understanding of the true flow field conditions experienced inside a velodrome. A developed understanding of these aerodynamic conditions will enable the flow field to be simulated more effectively in further wind tunnel or CFD-based research.

2. Cornering Theory

For this work, two right-handed Cartesian coordinate systems will be used. The first is a non-inertial body coordinate system (xyz) fixed in origin and orientation to the bicycle and cyclist system, as shown in Figure 1. Here the x axis is directed to the posterior of the cyclist, the y axis is directed to the cyclist's right and the z axis is directed upwards. The airflow experienced by a cyclist is composed of three components; u, v, w that correspond to the three primary axes x, y, z respectively. The second system is a ground-based inertial coordinate system (ijk) that is fixed with its origin at the centre of a velodrome. Here i is directed towards the centre of a straight, j is directed away from the centre of a bend, and k is directed upwards.

Figure 2 shows the steady-state cornering condition for a leaning cyclist turning at a constant speed around a level corner in still air. The cyclist rotates at a constant rotational velocity about an external point, the Centre of Rotation (CR), and the relative airflow is equal and opposite to the velocity of the Centre of Gravity (CG) of the cyclist. This results in curved airflow with a variation in the airflow angle and magnitude over the length of the cyclist and bicycle. Assuming an anti-clockwise corner, then anterior to the cyclist there will be an airflow angle (τ) in the horizontal (ij) plane. This airflow initially comes from the cyclist's left, transitions to a zero angle at the CG, and then exits towards the cyclist's left when it is posterior to the CG, as shown in Figure 2. As a cyclist leans during cornering, this angular airflow across the cyclist and bicycle results in both a yaw and a pitch angle. In addition to the change in direction, the magnitude of the airflow, and hence the dynamic pressure, will increase with radial distance from the CR. Due to the substantial lean angle of a track cyclist relative to the horizontal plane, this change in magnitude results in a slower air velocity at the top of the cyclist's body than at the wheels.

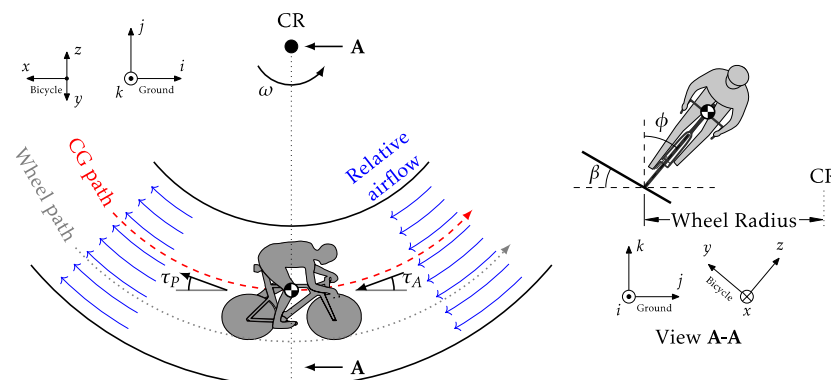


Figure 2. The steady-state airflow distribution observed by a leaning bicycle and cyclist on a corner of constant radius. Not to scale. Coordinate systems are shown displaced from their origin.

142 Shown in Figure 3 is the free-body-diagram of a steady-state cornering cyclist represented as a point mass.
 143 Representing a cyclist as a single point mass is a simplistic model as factors such as bicycle geometry, wheel
 144 path, rider size and rider position, can affect the validity of calculations, however it has been shown to provide
 145 a high level of accuracy (Fitton and Symons 2018) and as such will be used in this research.

146 When a cyclist traverses a bend, a centrifugal force ($F_C = mV_{CG}^2/R_{CG}$) acts radially outwards from the CR. This
 147 force produces a moment about the wheel base which is counteracted by the cyclist leaning into the corner
 148 and using their weight force ($F_W = mg$) to create a counter-moment to prevent the bicycle from tipping. Due
 149 to the flow curvature, there will be a horizontal aerodynamic force ($F_{A(\tau)}$), acting at the centre of pressure
 150 (CP), that is dependent on the angle of airflow. Anterior to the CG, this force will be directed outwards from
 151 the CR and posterior to the CG it will be directed inwards, producing a clockwise yawing moment about the k
 152 axis. Additionally, due to the radial change in airflow magnitude, there is a higher mean pressure on the inward
 153 side of the cyclist than the outward side. This pressure difference will produce an aerodynamic force acting
 154 outwards from the centre of rotation ($F_{A(P)}$) (Keogh et al. 2016). The magnitude of $F_{A(P)}$ is small in comparison
 155 to F_C and is omitted for the following theoretical calculations.

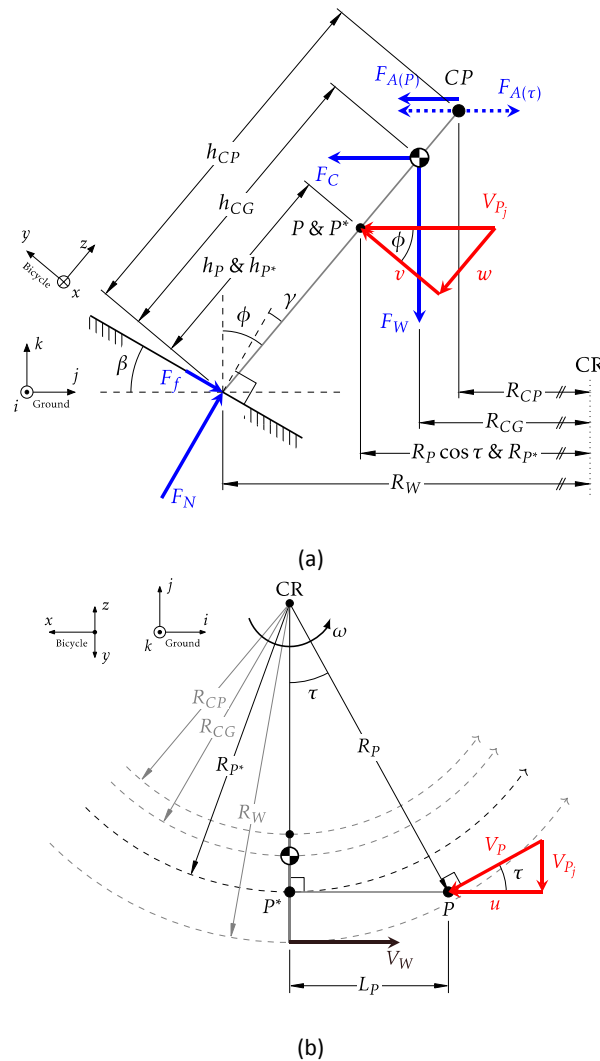


Figure 3. The steady-state free-body diagram of a bicycle traversing a level banked corner with the positions of the CR, CP, CG, P and P^* . (a) Front view showing the lean angle (ϕ), bank angle (β), wheel camber angle (γ) and various different turn radii. The force vectors in blue show the centrifugal force (F_C), weight force (F_W), aerodynamic force due to flow curvature ($F_{A(\tau)}$), aerodynamic force due to radial pressure ($F_{A(P)}$), normal force (F_N) and tyre friction force (F_f). The airflow velocity vectors in red show the bicycle-coordinate relative velocity components (v & w) that compose the lateral velocity (V_{Pj}) due to cornering. (b) Plan view showing the velocity of the wheels (V_W) and the different turn radii about the centre of rotation. The velocity of the probe (V_P) is composed of u and V_{Pj} and acts normal to the line between P and CR.

Due to the lean of the bicycle, the radius of the CG (R_{CG}) is less than the radius of the wheel/track contact point (R_W). Assuming that the turn radius of the wheels equals the radius of the black line on the velodrome track and if the height of the CG (h_{CG}) is known, then the lean angle (ϕ) for a given wheel velocity V_W can be calculated using Equation 1. This equation is implicit in ϕ and so requires an iterative method to solve, however it converges to 99% of its final value in less than 3 iterations.

$$\tan \phi = \frac{V_W^2 (R_W - h_{CG} \sin \phi)}{g R_W^2} \quad (1)$$

Figure 3 defines point P , a horizontal distance L_P anterior to the CG and a distance h_P above the wheelbase, and point P^* , the intersection of a horizontal line through P and a line from the CG to the ground. The points P and P^* have the same angular velocity but with turn radii of R_P and R_{P^*} respectively. As such there is a component of cross-flow (V_{Pj}) at point P which induces a yawed and pitched airflow relative to the bicycle. The cross-flow angle in the horizontal (ij) plane can be calculated with

$$\tan \tau = \frac{L_P}{R_W - h_P \sin \phi}. \quad (2)$$

and the velocity at P can be calculated by

$$V_P = \frac{V_W}{R_W} \sqrt{L_P^2 + (R_W - h_P \sin \phi)^2}. \quad (3)$$

The yaw angle can then be calculated with

$$\psi = \tan^{-1} \frac{v}{u} = \tan^{-1} (\tan \tau \cos \phi), \quad (4)$$

and the pitch angle by

$$\theta = \tan^{-1} \frac{-w}{u} = \tan^{-1} (-\tan \tau \sin \phi). \quad (5)$$

Inputting values to be used later in this paper, for a cyclist travelling at $V_W = 14.7$ m/s with $R_W = 22.5$ m, $h_{CG} = 1$ m, $h_P = 0.660$ m, and $L_P = 0.9$ m this equates to $V_P = 14.4$ m/s, $\psi = 1.7^\circ$, and $\theta = -1.6^\circ$ in the centre of the bends and $V_P = V_W$, $\psi = \theta = 0^\circ$ in the straights. Details of the track geometry and h_P were directly measured, while h_{CG} and L_P were estimated from cyclist body measurements.

An experimental test was conducted to measure the airflow on a bicycle ridden around a velodrome. The measurements were taken at the point P with a probe fixed to the frame of the bicycle so that it moved with the bicycle coordinate system and measured the air velocity relative to the cyclist.

3. Methods

Data was collected using a four-hole pressure probe (45 m/s, 150 Hz, Cobra probe, TFI, Australia) that measures the three components of velocity. This was fixed to an aluminium arm cantilevered anterior to the head tube of a generic track bicycle (size medium Pista, Hillbrick, Australia) and was used to measure the airflow relative to the bicycle in the body-centred xyz coordinate system. A reference static pressure was supplied to the Cobra probe via a static pressure probe attached to the forward component of the aluminium arm. The forward limit of the Cobra probe and static port were constrained by remaining behind the leading edge of the wheel to ensure the bicycle did not impact with another bicycle during team pursuit transitions. Two Hall-effect sensors were attached to the frame with a corresponding magnet on the rear wheel and the left crank arm to measure the wheel-speed and a pedal cadence respectively. The velocity probe and Hall-effect sensors were sampled at a frequency of 1250 Hz and were controlled by a TFI Data Acquisition System (DAQ) and laptop that was carried in a backpack by the rider. The total mass of the instruments was

188 approximately 4 kg and the bicycle setup for testing is shown in Figure 4. The position of the Hall-effect sensor
 189 on the frame was known and by assuming a constant rotational velocity of the cranks during a single pedal
 190 cycle the leg position at any point in the cycle was estimated.

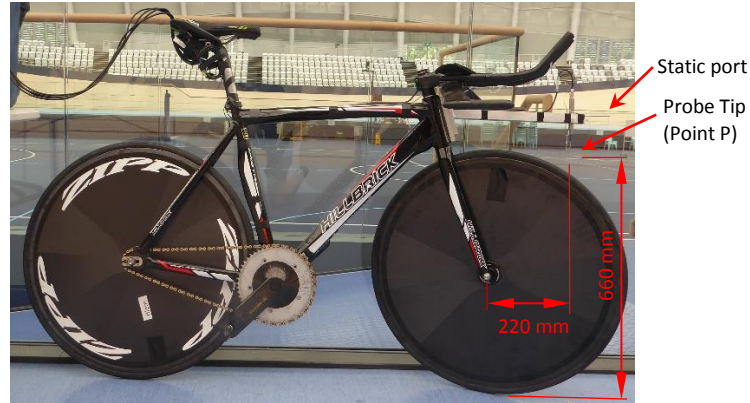


Figure 4. The instrumented bicycle with the position of the probe tip.

191 Stationary testing of the instrumented bicycle was completed at the University of Adelaide Thebarton wind
 192 tunnel. This is a closed-return wind tunnel with a cross sectional area of 2.75 m x 2 m, a maximum speed of
 193 30 m/s and turbulence intensity <0.5%. The bicycle was held on a fixed stand in the tunnel and tested with the
 194 probe in position with no rider, a rider sitting still, and a pedalling rider; all in conditions of 0° yaw.

195 On-track testing took place at the Adelaide Super-Drome, a 250 m indoor velodrome with bends of a maximum
 196 bank angle of 43° and minimum turn radius of 22.5 m. Four international-level elite male cyclists were used in
 197 this testing. The athletes provided informed consent and testing was conducted according to the University of
 198 Adelaide Human Research Ethics Committee guidelines. The first athlete rode the instrumented bicycle whilst
 199 the other three athletes rode their typical track bicycle. The athletes assumed their typical riding posture and
 200 rode in a team pursuit formation for 16 laps (4000 m) from a standing start in simulation of a competitive
 201 event. The team changed position every two laps so that data was collected twice at every position along the
 202 team line. The athlete on the instrumented bicycle led out the team in position 1 at the start of the race. Over
 203 the final 50 m the team abandoned the strict linear formation and the leading three riders spread out across
 204 the track to cross the pursuit line, in simulation of a competitive finish. The testing was filmed using a high-
 205 definition camera at 50 frames per second and the timestamp visually synchronised with the velocity probe
 206 data to find lap and position change times. Two races were completed with identical conditions, both
 207 producing very similar results indicating repeatability and confirming the results, with one of the tests detailed
 208 in this article.

209 The flow measured by the velocity probe was found to be highly periodic and hence the measured velocity
 210 components were split into their periodic and turbulent components by

$$f(t) = \langle f \rangle + f' \quad (6)$$

211 for $f = u, v, w, \psi, \theta$ (Hussain and Reynolds 1970). Here $\langle f \rangle$ is the phase average value of the flow at a given
 212 time t and f' is the turbulent velocity fluctuation at t . Two different phase average timeseries were obtained
 213 by twice applying a Savitzky-Golay filter with a quartic polynomial and two different window sizes for laps 2-
 214 16 (Savitzky and Golay 1964). The first lap was omitted as it was an acceleration phase. The first window is
 215 equal to the mean pedal cycle period of 0.56 s (108 rpm) and the second window is equal to the mean lap time
 216 of 17.27 s. The principal turbulence intensity was then calculated by the turbulent variation of the flow about
 217 the phase-averaged value with

$$I_{uvw} = \frac{\sqrt{\frac{1}{3}((u-\langle u \rangle)^2 + (v-\langle v \rangle)^2 + (w-\langle w \rangle)^2)}}{\bar{V}_P} \quad (7)$$

The alignment of the pressure probe to the bicycle coordinate system provides the greatest source of error in this experiment and has the potential to affect the absolute values of yaw and pitch. The probe was mounted to an aluminium arm cantilevered out from the head tube of the bicycle and aligned parallel to the bicycle and level. To align the probe, the bicycle was first geometrically aligned along the centreline of the University of Adelaide's 0.5 m x 0.5 m wind tunnel. This tunnel is far smaller than the bicycle, however it provided ease of alignment and the probe tip was encased in a low turbulence, well-conditioned airflow, unaffected by the asymmetric crankset and chain drive. The yaw angle of the probe was then aligned with the flow and marked in position with several scribe marks which were used to realign the probe before in-field testing at the velodrome. The pitch angle was dependent on the trueness of the hole in the cantilever arm and the level of the arm relative to the ground. The probe was removed from the bicycle and replaced in the wind tunnel multiple times to determine the accuracy of this method. A conservative estimate for maximum absolute error in yaw and pitch for placement of the probe is $<2^\circ$. The effect of this error would be to linearly translate the results by the misalignment of the probe and would not alter the relative changes in yaw and pitch observed during a test. The probe manufacturers claim an accuracy of ± 0.3 m/s and $\pm 1.0^\circ$ for the flow range of 2-45 m/s in a $\pm 45^\circ$ cone.

4. Results and Discussion

4.1. Stationary wind tunnel testing

Stationary testing conducted in the 2.75 m x 2 m Thebarton wind tunnel showed a deceleration of the air velocity at the probe tip, shown in Table 1 for V_P/V_T where V_P is the measured probe velocity and V_T is the free-stream velocity of the tunnel measured by a pitot-static tube. This upstream disturbance can be seen to be partly due to the bicycle only and partly due to the influence of the rider. The yaw angle of 1.2 - 1.4° is due to misalignment of the probe or asymmetries in the flow and bicycle. The pitch angle of 4.63° with no rider is likely due to these same factors in addition to the presence of the front wheel which causes an upwards deflection of the flow. When the rider is present there is a decrease in the pitch angle of 1.8° due to the upstream influence of the rider's arms and hands turning the airflow down towards the ground.

Table 1. Summary of data from stationary testing of the instrumented bicycle (Mean \pm Standard Deviation). Values are obtained by averaging results across tunnel velocities of 9, 11, 13, and 15 m/s.

Rider	V_P/V_T	I_{uvw} [%]	ψ [$^\circ$]	θ [$^\circ$]
None	0.979 ± 0.0020	0.276 ± 0.037	1.19 ± 0.02	4.63 ± 0.07
Still	0.956 ± 0.0004	0.269 ± 0.020	1.19 ± 0.04	2.82 ± 0.05
Pedalling	0.954 ± 0.0021	0.775 ± 0.284	1.39 ± 0.02	2.83 ± 0.04

In order to observe if there were any periodic components to the airflow a Fourier transform was applied to the three principal components of velocity, shown in Figure 5 for both a rider sitting still (cranks horizontal) and a rider pedalling. In these graphs there is a distinct spectral peak at 3.8 Hz for the u component that is also seen when no rider is present (not shown) and is likely due to a perturbation in the tunnel flow. There is an unknown frequency at 93.7 Hz that is also observable in the velocity data obtained on the track, the cause of which is unknown but could be due to vibration in the probe or bicycle frame.

There is a relative airflow periodic dependence on the rider's cadence, with a peak in the yaw that matches the cadence frequency and peaks at approximately twice the cadence frequency in the total velocity and pitch. This periodic motion is hypothesised to be due to the upstream influence of the rider's legs. During each pedal cycle, one leg will be forwards while the other is rearwards, producing an asymmetric upstream effect which induces a periodic yaw angle fluctuation. As one leg produces a positive ψ and the other a negative, the yaw period matches the cadence period. However, the V and θ periodicity are likely due to the forward and vertical motion of each leg and, as these are independent of a particular leg, their period is twice the cadence

258 frequency. Whilst these periodic motions are observed, their amplitudes are small (<0.01 m/s and $<0.08^\circ$), not
 259 greatly above the background turbulence, and hence are likely to have minimal impact on a cyclist.

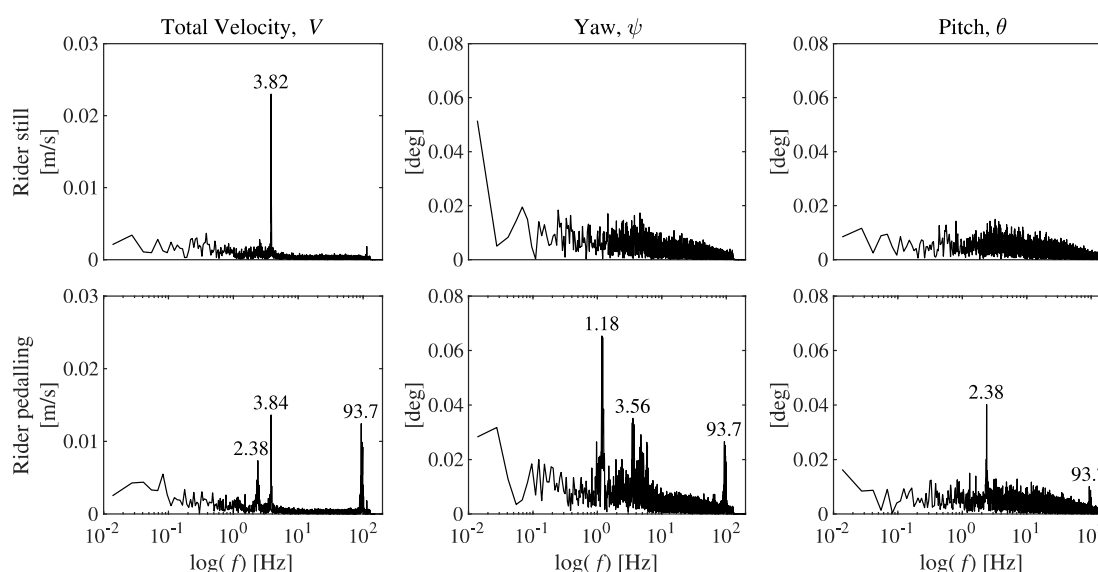


Figure 5. The Fourier Transform of the three components of velocity (u, v, w) for stationary testing completed in the wind tunnel at a free-stream velocity of 15.0 m/s. The top row is when the rider is sitting still on the bicycle and the bottom row is when the rider is pedalling at an average cadence of 1.20 ± 0.03 Hz (71.7 ± 1.8 rpm). Notable frequencies are labelled.

260 4.2. Velodrome testing

261 The velodrome testing results indicate that the airflow is highly variant and dependent on three main factors,
 262 listed in order of relative magnitude; the rider's position in the team line, their location on the track, and the
 263 point in their cadence cycle. Displayed in Figure 6 are the three components of air velocity and the wheel
 264 speed for the duration of the 16-lap test, showing the clear differences due to position in the team.

265 A useful metric for this testing is the ratio between the probe velocity and the wheel velocity, V_P/V_W . This
 266 represents the relationship between the airflow experienced by the cyclist and their speed over the track. This
 267 ratio can be observed in Figure 6 by the difference in speed between u and V_W for position 1. In an ideal
 268 environment V_P/V_W should be unity, but there are a number of factors that influence this. The most significant
 269 contribution arises from the upstream disturbance of the bicycle and cyclist slowing the airflow at the probe
 270 tip. A summary of stationary testing completed in the 2.75 m x 2 m wind tunnel, shown in Table 1,
 271 demonstrates the deceleration of the air velocity at the probe tip. This deceleration of the airflow ahead of
 272 the rider has been previously reported by Blocken et al. (2018b) who used Computational Fluid Dynamics (CFD)
 273 calculations to measure the streamwise component of airflow at three different distances ahead of a cyclist
 274 in a peloton at 15 m/s and across the full height of a cyclist in the sagittal plane. The mean value for each
 275 distance was plotted and for the rider at the front in clear airflow $V_P/V_W = 0.97$. The distances of the planes
 276 ahead of the rider are not presented; however, they are likely to be further ahead of the rider than P and so
 277 the airspeed deceleration at P is likely to be greater. A second difference between V_P and V_W is seen in the
 278 earlier theoretical calculations which predicted $V_P/V_W = 0.98$ due to the faster speed at the wheels than P
 279 when on the bends.

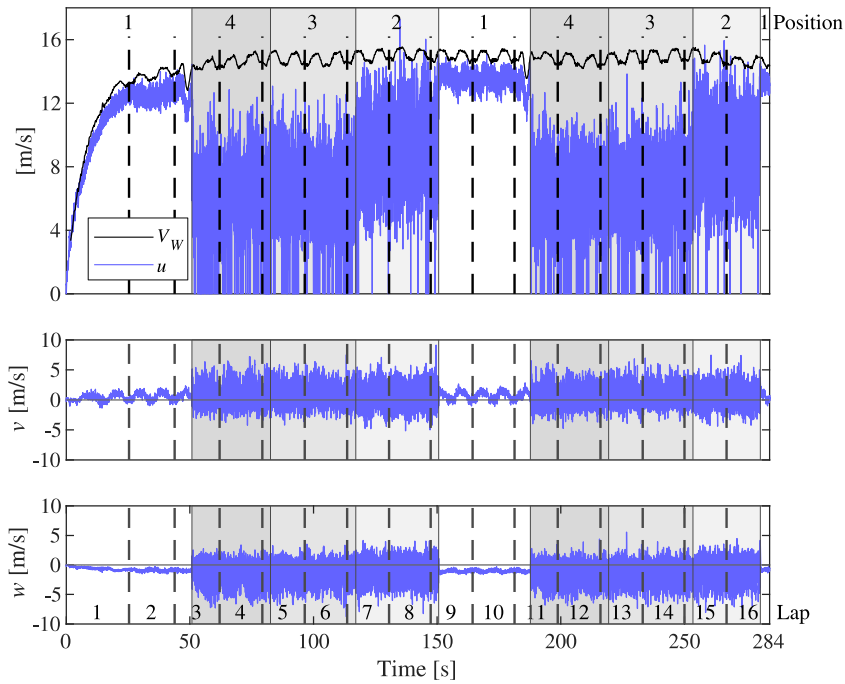


Figure 6. The three components of air velocity as well as the wheel speed for the length of a simulated team pursuit race. Lap markers are indicated by the dashed vertical lines and the bottom numbers 1 to 16. The bicycle's position along the team line is indicated by the shaded areas and the top numbers 1 to 4.

4.3. Effect of rider position

Observing Figure 6, the clearest trends are seen in the effect of rider position on the three components of air velocity. When the cyclist is in position 1, they are leading the team and the magnitude of the air velocity is relatively close to the wheel speed. However, when they move to the rear of the team pursuit line in position 4, the headwind is much lower than the wheel speed and the turbulence intensity greatly increases: values are provided in Table 2. This is due to the cyclist riding in the wake/s of the three preceding riders who produce highly turbulent and attenuated airflow. As the next rider changes position and the instrumented bicycle moves to position 3, there is minimal difference in the air velocity and turbulence intensity compared to position 4. After the third transition, when the instrumented bicycle is in position 2, there is a clear difference to both positions 3/4 and 1. In position 2 there is still a high turbulence intensity and the air velocity is lower than when they are at position 1, but not as low as positions 3 or 4. This demonstrates that the wake from the leading cyclist compounds with that of the second cyclist to retard the airflow further for the third and fourth cyclists. This is also seen in the increase in the pitch angle through positions 1 to 4, indicating that the downwash from each rider compounds to further increase the downwards airflow as measured by the following rider. However, after three riders the effect of a change between positions plateaus and the pitch angle and turbulence intensity increase at a slower rate.

The observed change in the airflow between different positions along the team pursuit line is similar to previous work in the literature on the relative drag force experienced at different positions in the line, as shown in Table 2. The drag force for a rider in a given position along the line is provided relative to the drag of that rider on their own by F_{pos}/F_i where F_{pos} is the drag of the cyclist in a given position and F_i is the drag of the same rider on their own. From Table 2 it can be seen that the drag reduction increases from first to third position before plateauing from third to fourth position, mirroring the relative airflow observed in the present experiment. The cause of this drag reduction is the greatly reduced dynamic pressure in the wake of the preceding cyclist, shown here as a reduction in V_p for each subsequent rider. This work cannot provide an

accurate indication of the drag force as only a single point of the flow experienced by a cyclist was measured; however, it provides a simple indication of the expected flow field.

Table 2. Average aerodynamic factors at each position along the team pursuit line from this study (Mean \pm Standard Deviation) and F_{pos}/F_i for each position along the line from a) wind tunnel testing (Barry et al. 2015), b) CFD testing (Blocken et al. 2018b), c) CFD testing (Blocken et al. 2018a), and d) in-situ velodrome testing (Fitton et al. 2018). Position 1 includes the acceleration phase.

Position	1 (Front)	2	3	4 (Rear)
$V_W [ms^{-1}]$	13.20 ± 2.76	14.91 ± 0.33	14.87 ± 0.31	14.67 ± 0.31
$V_P [ms^{-1}]$	12.10 ± 2.46	9.33 ± 1.81	7.06 ± 1.56	6.72 ± 1.62
Yaw, $\psi [^\circ]$ (Straights)	0.68 ± 2.72	1.35 ± 8.81	4.25 ± 10.46	2.69 ± 11.01
Yaw, $\psi [^\circ]$ (Bends)	4.18 ± 2.55	5.76 ± 8.29	8.04 ± 10.08	6.98 ± 11.62
Pitch, $\theta [^\circ]$ (Straights)	-1.47 ± 0.93	-2.94 ± 8.96	-5.15 ± 11.09	-6.52 ± 11.70
Pitch, $\theta [^\circ]$ (Bends)	-2.2 ± 0.86	-4.43 ± 8.71	-8.67 ± 10.70	-9.87 ± 11.73
$I_{uvw} [\%]$ (Cadence)	1.5	14.9	17.3	18.5
$I_{uvw} [\%]$ (Lap)	3.2	16.1	19.0	20.3
V_P/V_W	0.92	0.63	0.47	0.46
F_{pos}/F_i^a	0.95	0.55	0.45	0.43
F_{pos}/F_i^b	0.98	0.59	0.50	0.46
F_{pos}/F_i^c	0.98	0.62	0.50	0.47
F_{pos}/F_i^d	0.96	0.58	0.52	0.53

4.4. Effect of location on the track

There is a significant dependence of the airflow on the cyclist's location around the track that is clearly evident when observing the yaw and pitch angles during a lap with the instrumented bicycle in position 1, shown in Figure 7 for lap 10. The yaw and pitch angles are highly periodic in nature, with a clear dependence on both the turn location and cadence cycle. Shown in Table 2 are the yaw and pitch angles for each of the four positions, split into the averages for when the cyclist is on the straights and the bends. When the cyclist is turning around the bend, a significant increase in the yaw angle, an increase in the pitch angle magnitude, and a minor increase in the wheel speed is observed.

The increase in the yaw angle is much greater than the theoretically calculated value of 1.7° (Equation 4) and could be due to a variety of factors. When cornering, the cyclist will steer the front wheel into the bend and the large surface of the disk wheel would induce a positive yaw angle at the probe tip. Additionally, due to the cyclist riding in a curved flow field rather than a straight headwind, the stagnation point would move from directly anterior to partially around to the left, inducing a positive yaw angle at the position of the probe.

Close examination of Figure 7 shows that the yaw angle undergoes a rapid change at the entries and exits of the bends. At these locations on the track the rider undergoes a transition from an upright position ($\phi = 0$) to a lean angle of approximately 40° and then back when exiting. Thus, the rider will experience a roll-induced yaw at these locations. The roll-induced yaw will vary from zero at the track surface to a maximum at the rider's head and shoulders, and at the probe height this equates to approximately $2-4^\circ$.

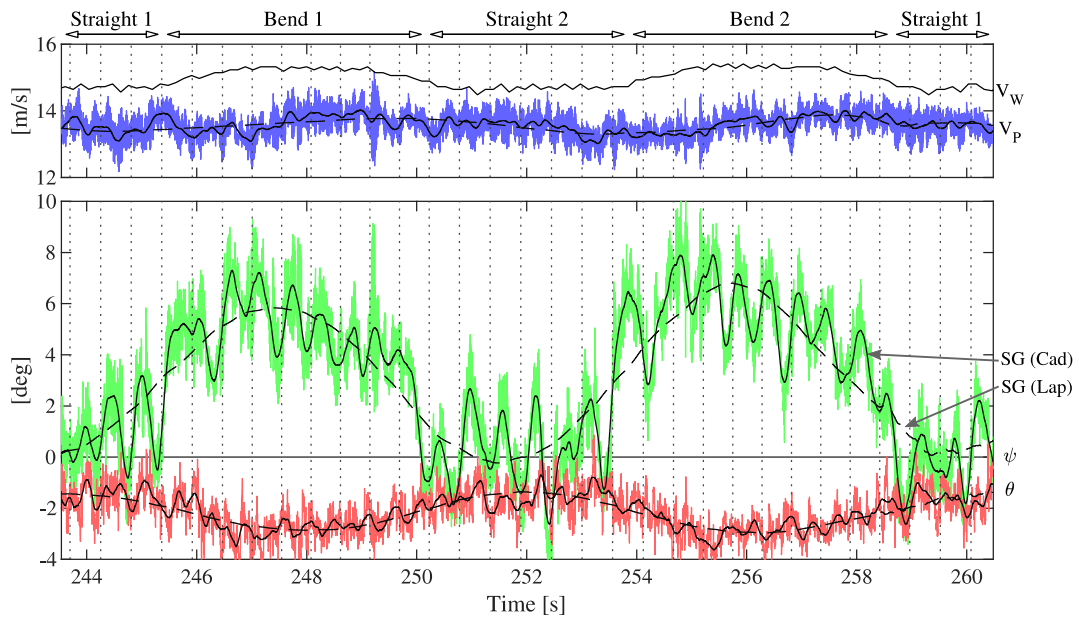


Figure 7. Velocity of the wheels (V_W), total velocity (V_P), yaw (ψ) and pitch (θ) over the course of a single lap (Lap 10, position 1). The solid black lines represent the Savitzky-Golay filtered data with a window size equal to the cadence period and the dashed black lines are the filter with a window size equal to half of the lap time. Vertical dotted lines are indications of when the left leg is at top-dead-centre (TDC).

327 In order to better visually display the effect of track location on the yaw and pitch angles, a novel method of
 328 displaying the results has been developed and is shown in Figure 8. This velodrome plot is based on a number
 329 of assumptions and as such is only to be used for qualitative purposes in identifying the major trends. It is
 330 produced by approximating the track as two straights and two semicircles and assumes a constant wheel
 331 speed based on the lap time and track geometry. The yaw/pitch angle vs time data is then converted to
 332 yaw/pitch angle vs lap distance with the lap position shown by the solid black line and the angular magnitude
 333 represented by the radial distance from that line. This graph clearly shows the correlation between the yaw
 334 and pitch angles and the cyclist's position on the bends and straights. Also shown is the data from the second
 335 test which can be seen to follow a very similar trend to the first test.

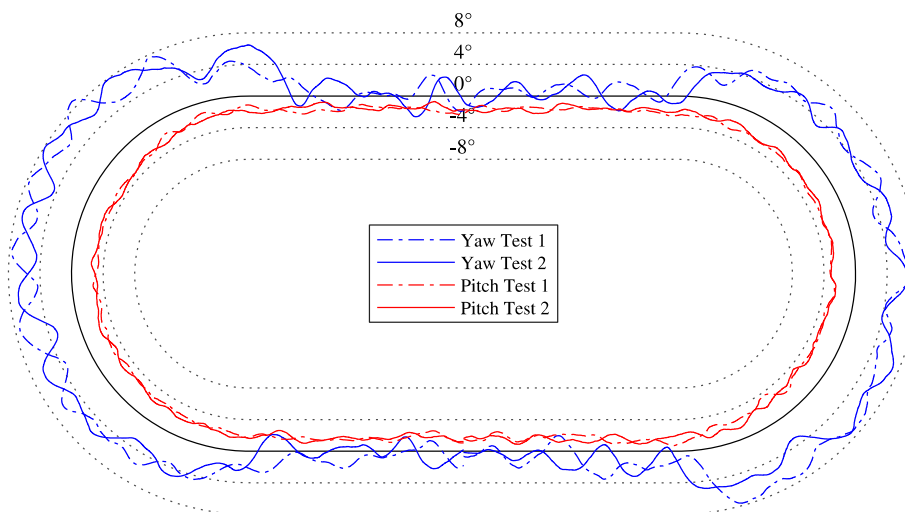


Figure 8. The cadence-filtered yaw and pitch angles for lap 10, when the cyclist is in position 1, from both tests, displayed in a velodrome plot.

336 In order to further investigate the cyclic nature of the velocity field, a Fourier transform was applied to the
 337 yaw and pitch data, excluding the first lap which was an acceleration phase, and the results are shown in Figure

338 9. In this figure two clear peaks in the yaw angle signal and a single peak in the pitch angle signal can be
 339 observed. The first peak in the yaw angle and the peak in the pitch angle occur at a frequency of 0.116 Hz
 340 which corresponds to a lap time of 17.271 s. The mean lap time for laps 2 to 16 was 17.273 s, a 0.01%
 341 difference, showing a clear dependence of the yaw and pitch angles on the bank angle and turn radius. There
 342 are also two minor peaks after the cadence peak which are at twice and three times the cadence frequency.

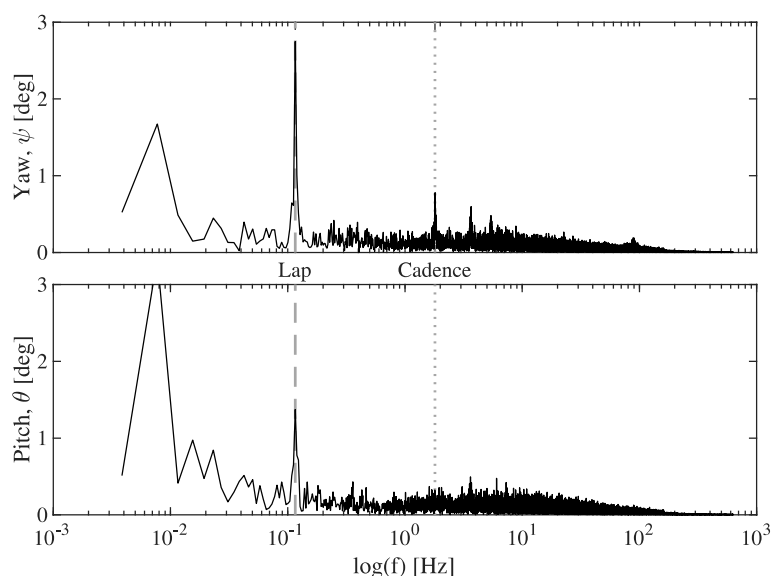


Figure 9. Fourier transform of the yaw (ψ) and pitch (θ) angles for laps 2 to 16. The dashed line indicates the measured mean half-lap frequency of 0.116 Hz, and the dotted line indicates the measured mean cadence frequency of 1.80 Hz (108.0 rpm).

343 4.5. Effect of pedal cycle

344 The above measurements demonstrate that a significant component of the airflow unsteadiness is related to
 345 the cyclist's pedalling cadence with a periodic change in yaw angle that closely follows the cadence frequency.
 346 This is clearly seen in the filtered yaw angle from Figure 7 where a small-amplitude and high-frequency wave
 347 from the cadence cycle is overlaid on top of a high-amplitude and low-frequency wave from the lap cycle. A
 348 periodicity can also be visually observed that matches the cadence markers.

349 The second peak in the Fourier transform of the yaw signal in Figure 9 has a frequency of 1.81 Hz which
 350 corresponds to a cadence of 108.6 rpm, a difference <0.6% from the measured mean cadence of 108.0 rpm,
 351 implying a clear dependence of the yaw angle on the leg position. The amplitude of this oscillation is 2.75°
 352 which is much greater than the 0.07° observed in the wind tunnel, indicating the influence of a secondary
 353 factor. The local peak in the yaw angle was estimated to occur when the left leg is 120° forward of top-dead-
 354 centre (TDC). Of note is that there is no clear dependence of the pitch angle on the cadence cycle from on-track
 355 testing.

356 The cause of the variation in yaw angle due to the cadence cycle is unknown but it is proposed that it arises
 357 due to rocking and weaving of the bicycle as the cyclist pedals. The local maximum in the yaw angle occurs at
 358 an approximate leg position of 120° which is just past the centre of the power stroke for the right leg. As a
 359 cyclist pushes down with their right leg, the bicycle rocks to the left, sweeping the probe tip laterally right to
 360 left, inducing a positive yaw angle with a maximum value at the centre of the power stroke when the bicycle
 361 is rocking at the greatest velocity. This process is then mirrored in the second half of the pedal cycle, producing
 362 a low magnitude sinusoidal yaw angle of frequency equal to that of the pedal cycle. Preliminary investigations
 363 in the 2.75 m x 2 m wind tunnel qualitatively support this hypothesis and further research would require
 364 measuring the crank angle at a higher resolution and recording both the steering angle and the roll angle of
 365 the bicycle.

The turbulence intensity has been calculated twice using the filtered signal with both the lap and cadence windows, as shown in Table 2. This, combined with the turbulence intensity measured in the wind tunnel, can be used to differentiate the causes of turbulence. By subtracting $I_{uvw}(\text{Cadence})$ from $I_{uvw}(\text{Lap})$ the turbulence intensity due to only the cyclists' cadence is found to be 1.2%. From the wind tunnel testing, it was observed that the pedalling motion produced a turbulence intensity of 0.5% above the background tunnel turbulence. As such, it can be seen that the turbulence associated with the periodic velocity fluctuations due to pedalling can be partially attributed to the movement of the legs and partially due to other factors. This has an impact on wind tunnel or CFD investigations where the background turbulence is required to be simulated.

4.6. General Discussion

The data acquisition system contained in the backpack could influence the results through two different methods. Firstly, the added mass on top of the rider's back would slightly alter the position of the centre of gravity, thereby changing the expected yaw and pitch values due to an altered lean angle. This effect was calculated with Equations 1-5 and a 10% change in centre of gravity height, much more than possible from the backpack, produces a <0.2% change in yaw and pitch angles. Secondly, the size and shape of the backpack could have an upstream aerodynamic effect at the probe tip. The influence of this is expected to be minimal due to the much larger body of the cyclist between the backpack and the probe producing the greatest upstream aerodynamic influence. In order to qualitatively assess this behaviour, a test was conducted at a later date with the data acquisition equipment contained on a pannier rack behind the rider and a 'dummy' backpack on the rider's back. The cyclist then rode a number of laps around an empty velodrome both with and without the backpack and no difference was observed in any of the recorded data.

Collating the data obtained over the length of the simulated race, a discrete Probability Density Function (PDF) was produced by binning the data into 1° increments and calculating the probability of each bin value occurring over the length of the data. This details the probability of a certain yaw or pitch angle occurring during riding and is shown in Figure 10, split into the four team pursuit positions. The results of the PDF demonstrate an approximate normal distribution of airflow angles experienced during track cycling. When a cyclist is in position 1, the airflow is relatively constant in direction with a small range of yaw and minimal range of pitch angles, exemplified by a very narrow distribution. However when the cyclist is in positions 2 to 4, the range of yaw and pitch angles increases and the distribution flattens. The obtained PDFs can be used for drag reduction testing in a similar manner to Wind Averaged Drag (Brownlie et al. 2010, Barry 2018) where the measured drag at a certain yaw angle is weighted according to the probability of that yaw angle occurring. This provides a simple comparison between otherwise difficult to distinguish drag results.

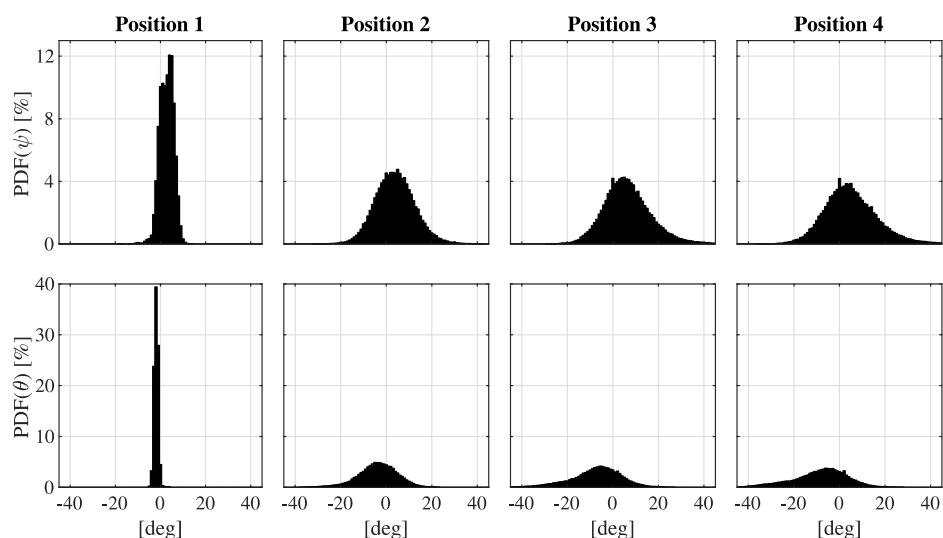


Figure 10. Probability Density Function (PDF) of the yaw and pitch angles.

398 5. Conclusion

399 In this experimental investigation, the air velocity at a single point anterior to a cyclist was recorded for the
400 length of a simulated team pursuit race. The results indicated a significant dependence of the airflow on three
401 primary factors; the cyclist's position in the team pursuit line, their location around the track, and their
402 cadence cycle. When the cyclist is at the front of the team pursuit line, the airflow magnitude is 92% of the
403 wheel speed with a turbulence intensity of 1.5%, however when the cyclist moves position and into the wake
404 of three other riders, the velocity ratio drops to 46% and the turbulence intensity increases significantly to
405 18.5% for the final position along the team pursuit line. This drop in velocity ratio provides a significant
406 lowering of the dynamic pressure, and hence the drag, experienced by the cyclists along the team pursuit line
407 and follows a similar pattern to previously reported team pursuit line drag ratios.

408 In addition, it is clear that the effects of cornering have a major influence on the airflow incident on a cyclist.
409 The experimental results display a yaw angle ranging from -2° to 8° and a pitch angle range of -1° to -3° , which
410 are much greater than the theoretically calculated maximum yaw and pitch values of 1.7° and -1.6°
411 respectively. It is also clear that the pedalling motion induces a yaw angle fluctuation on the rider and is this
412 likely due to rocking and weaving of the bicycle. The experiments conducted in this investigation develop our
413 understanding of the flow field experienced during track cycling and a team pursuit event in particular. This
414 can be used in the advancement of wind tunnel or CFD testing through replication of turbulence and flow
415 angles, providing a more realistic environment for experimentation.

416 **Acknowledgements:** The authors would like to acknowledge the support of the Australian Institute of Sport
417 and the South Australian Sports Institute.

418 6. References

- 419 Barry, N. (2018). 'A New Method for Analysing the Effect of Environmental Wind on Real World
420 Aerodynamic Performance in Cycling', *Proceedings* **2**(6): 211 DOI: doi:10.3390/proceedings2060211
- 421 Barry, N., D. Burton, T. Crouch, J. Sheridan and R. Luescher (2012). 'Effect of crosswinds and wheel
422 selection on the aerodynamic behavior of a cyclist', *Procedia Engineering* **34**: 20-25 DOI:
423 <https://doi.org/10.1016/j.proeng.2012.04.005>
- 424 Barry, N., D. Burton, J. Sheridan, M. Thompson and N. A. T. Brown (2015). 'Aerodynamic drag
425 interactions between cyclists in a team pursuit', *Sports Engineering* **18**(2): 93-103 DOI:
426 10.1007/s12283-015-0172-8
- 427 Barry, N., D. Burton, J. Sheridan, M. Thompson and N. A. T. Brown (2016). 'Flow field interactions
428 between two tandem cyclists', *Experiments in Fluids* **57**(12): 181 DOI:
429 <https://doi.org/10.1007/s00348-016-2273-y>
- 430 Belloli, M., S. Giappino, F. Robustelli and C. Somaschini (2016). 'Drafting Effect in Cycling:
431 Investigation by Wind Tunnel Tests', *Procedia Engineering* **147**: 38-43 DOI:
432 <https://doi.org/10.1016/j.proeng.2016.06.186>
- 433 Blocken, B., T. Defraeye, E. Koninckx, J. Carmeliet and P. Hespel (2013). 'CFD simulations of the
434 aerodynamic drag of two drafting cyclists', *Computers & Fluids* **71**: 435-445 DOI:
435 <https://doi.org/10.1016/j.compfluid.2012.11.012>
- 436 Blocken, B., Y. Toparlar, T. van Druenen and T. Andrianne (2018a). 'Aerodynamic drag in cycling team
437 time trials', *Journal of Wind Engineering and Industrial Aerodynamics* **182**: 128-145 DOI:
438 <https://doi.org/10.1016/j.jweia.2018.09.015>
- 439 Blocken, B., T. van Druenen, Y. Toparlar, F. Malizia, P. Mannion, T. Andrianne, T. Marchal, G.-J. Maas
440 and J. Diepens (2018b). 'Aerodynamic drag in cycling pelotons: New insights by CFD simulation and
441 wind tunnel testing', *Journal of Wind Engineering and Industrial Aerodynamics* **179**: 319-337 DOI:
442 10.1016/j.jweia.2018.06.011
- 443 Brownlie, L., P. Ostafichuk, E. Tews, H. Muller, E. Briggs and K. Franks (2010). 'The wind-averaged
444 aerodynamic drag of competitive time trial cycling helmets', *Procedia Engineering* **2**(2): 2419-2424
445 DOI: 10.1016/j.proeng.2010.04.009
- 446 Caddy, O., W. Fitton, D. Symons, A. Purnell and D. Gordon (2017). 'The effects of forward rotation of
447 posture on computer-simulated 4-km track cycling: Implications of Union Cycliste Internationale rule
448 1.3.013', *Proceedings of the Institution of Mechanical Engineers, Part P: Journal of Sports Engineering
449 and Technology* **231**(1): 3-13 DOI: 10.1177/1754337115619306
- 450 Cooper, K. R. and S. Watkins (2007). 'The Unsteady Wind Environment of Road Vehicles, Part One: A
451 Review of the On-road Turbulent Wind Environment', *SAE International* DOI:
452 <https://doi.org/10.4271/2007-01-1236>

453 Crouch, T. N., D. Burton, N. A. T. Brown, M. C. Thompson and J. Sheridan (2014). 'Flow topology in
 454 the wake of a cyclist and its effect on aerodynamic drag', *Journal of Fluid Mechanics* **748**: 5-35 DOI:
 455 <https://doi.org/10.1017/jfm.2013.678>

456 Crouch, T. N., D. Burton, Z. A. LaBry and K. B. Blair (2017). 'Riding against the wind: a review of
 457 competition cycling aerodynamics', *Sports Engineering* **20**(2): 81-110 DOI: 10.1007/s12283-017-
 458 0234-1

459 Crouch, T. N., D. Burton, M. C. Thompson, N. A. T. Brown and J. Sheridan (2016). 'Dynamic leg-motion
 460 and its effect on the aerodynamic performance of cyclists', *Journal of Fluids and Structures* **65**: 121-
 461 137 DOI: <https://doi.org/10.1016/j.jfluidstructs.2016.05.007>

462 D'Auteuil, A. (2010). 'Manipulation of the Boundary Layer Transition to Enhance the Aerodynamic
 463 Performance of Athletes', Ottawa-Carleton Institute for Mechanical and Aerospace Engineering DOI:
 464 <https://doi.org/10.22215/etd/2010-12529>.

465 D'Auteuil, A., G. L. Larose and S. J. Zan (2012). 'Wind turbulence in speed skating: Measurement,
 466 simulation and its effect on aerodynamic drag', *Journal of Wind Engineering and Industrial
 467 Aerodynamics* **104**: 585-593 DOI: 10.1016/j.jweia.2012.02.002

468 Defraeye, T., B. Blocken, E. Koninckx, P. Hespel, P. Verboven, B. Nicolai and J. Carmeliet (2014). 'Cyclist
 469 Drag in Team Pursuit: Influence of Cyclist Sequence, Stature, and Arm Spacing', *Journal of
 470 Biomechanical Engineering* **136** DOI: 10.1115/1.4025792

471 Fintelman, D. M., H. Hemida, M. Sterling and F. X. Li (2015). 'CFD simulations of the flow around a
 472 cyclist subjected to crosswinds', *Journal of Wind Engineering and Industrial Aerodynamics* **144**: 31-41
 473 DOI: <https://doi.org/10.1016/j.jweia.2015.05.009>

474 Fitton, B., O. Caddy and D. Symons (2018). 'The impact of relative athlete characteristics on the drag
 475 reductions caused by drafting when cycling in a velodrome', *Proceedings of the Institution of
 476 Mechanical Engineers, Part P: Journal of Sports Engineering and Technology* **232**(1): 39-49 DOI:
 477 10.1177/1754337117692280

478 Fitton, B. and D. Symons (2018). 'A mathematical model for simulating cycling: applied to track
 479 cycling', *Sports Engineering* **21**(4): 409-418 DOI: 10.1007/s12283-018-0283-0

480 Hussain, A. K. M. F. and W. C. Reynolds (1970). 'The mechanics of an organized wave in turbulent
 481 shear flow', *Journal of Fluid Mechanics* **41**(2): 241-258 DOI: 10.1017/S0022112070000605

482 Íñiguez-de-la-Torre, I. and J. Íñiguez (2005). 'Cycling and wind: does sidewind brake?', *European
 483 Journal of Physics* **27**(1): 71-74 DOI: 10.1088/0143-0807/27/1/007

484 Keogh, J., T. Barber, S. Diasinos and G. Doig (2016). 'The aerodynamic effects on a cornering Ahmed
 485 body', *Journal of Wind Engineering and Industrial Aerodynamics* **154**: 34-46 DOI:
 486 10.1016/j.jweia.2016.04.002

487 Kyle, C. R. (2003). 'Selecting Cycling Equipment', In: *High-tech cycling*, Ed. by E. Burke, 2, Human
 488 Kinetics, Champaign, USA.

489 Kyle, C. R. and E. R. Burke (1984). 'Improving the racing bicycle', *Mechanical Engineering* **106**(9): 34-
490 45

491 Lukes, R., J. Hart and S. Haake (2012). 'An analytical model for track cycling', *Proceedings of the*
492 *Institution of Mechanical Engineers, Part P: Journal of Sports Engineering and Technology* **226**(2): 143-
493 151 DOI: 10.1177/1754337111433242

494 Savitzky, A. and M. J. Golay (1964). 'Smoothing and differentiation of data by simplified least squares
495 procedures', *Analytical chemistry* **36**(8): 1627-1639 DOI: 10.1021/ac60214a047

496 Terra, W., A. Sciacchitano and Y. H. Shah (2019). 'Aerodynamic drag determination of a full-scale
497 cyclist mannequin from large-scale PTV measurements', *Experiments in Fluids* **60**(2): 29 DOI:
498 10.1007/s00348-019-2677-6

499 Underwood, L. (2012). 'Aerodynamics of Track Cycling' PhD Thesis, The University of Canterbury

500 Watkins, S. and F. Alam (2014). 'The Turbulent Flow Field Relevant to Outdoor Sports', *Procedia*
501 *Engineering* **72**: 792-797 DOI: <https://doi.org/10.1016/j.proeng.2014.06.134>

502